Elastic constants and orientational viscosities of a bent-core nematic liquid crystal

M. Majumdar,[1] P. Salamon,[2] A. Jákli,[3] J. T. Gleeson,[1] and S. Sprunt[1]
[1]*Department of Physics, Kent State University, Kent, Ohio 44242, USA*
[2]*Research Institute for Solid State Physics and Optics, Hungarian Academy of Sciences, H-1525 Budapest, Hungary*
[3]*Chemical Physics Interdisciplinary Program and Liquid Crystal Institute, Kent State University, Kent, Ohio 44242, USA*
(Received 23 September 2010; published 7 March 2011)

Using a combination of dynamic light scattering and Freedericksz transitions induced in applied magnetic and electric fields, we have determined the absolute magnitudes of the Frank elastic constants and effective orientational viscosities of the bent-core nematic liquid crystal, 4-chloro-1,3-phenylene bis 4-[4'-(9-decenyloxy)benzoyloxy] benzoate. At a fixed temperature 2 °C below the isotropic-nematic transition, we find $K_{11} = 3.1 \times 10^{-12}$ N, $K_{22} = 0.31 \times 10^{-12}$ N, $K_{33} = 0.88 \times 10^{-12}$ N, $\eta_{\text{splay}} = 1.1$ Pa s, $\eta_{\text{twist}} = 0.37$ Pa s, and $\eta_{\text{bend}} = 1.2$ Pa s. The unusual anisotropies of these parameters are discussed in terms of short-range, smectic-C-like correlations among molecules in the nematic phase.

DOI: 10.1103/PhysRevE.83.031701 PACS number(s): 61.30.−v, 72.80.Le

I. INTRODUCTION

Bent-core and other reduced symmetery molecules exhibiting liquid crystalline (LC) phases have opened up a major new dimension in the science of thermotropic LCs. Experiments on the nematic phase of bent-core LCs, in particular, have revealed a host of interesting properties, including giant flexoelectricity [1]; a significant Kerr effect [2]; induced [3] and spontaneous [4,5] biaxial orientational order; unusually large viscosity to elasticity ratios [6,7] and flow viscosity [8]; new electroconvection behavior [9]; and possible effects of higher orientational order parameters on the isotropic-nematic transition [10]. Meanwhile, theoretical investigations [11] have predicted that spontaneously chiral and even polar phases should be favored in bent-core nematics (BCNs)

Given this range of phenomena, much of which is clearly distinct from the behavior of calamitic (rodlike) nematics, it is imperative to establish such basic properties of BCNs as the magnitudes of the individual elastic constants and orientational viscosities associated with splay, twist, and bend deformations of the director field. Recent studies demonstrate that in certain BCNs, the anisotropy of the splay and bend elastic constants is reversed [12] from the usual case in calamitic thermotropics (where the splay constant K_{11} is less than the bend constant K_{33}, except in the immediate vicinity of a nematic-smectic transition) and that the temperature dependences of K_{11} and K_{33} in the nematic phase are somewhat anomalous [13]. There are also reports that the twist constant K_{22} may be substantially smaller than the other elasticities [14], and that K_{33} can be reduced by a factor of 2 or more by mixing bent-core molecules into calamitic nematic hosts [15]. However, to our knowledge, a complete set of values of the elastic constants and of the related phenomenological viscosities (η_{splay}, η_{twist}, and η_{bend}) is not yet available for a single BCN compound, and no adequate model, incorporating information about the nanostructure of BCNs (such as the nature of short-range smectic order), has been presented to account for the unconventional behavior of the elastic constants revealed in the previous studies.

In this contribution, we report absolute measurements of the elastic constants and orientational viscosities for the bent-core nematic compound 4-chloro-1,3-phenylene bis 4-[4′-(9-decenyloxy)benzoyloxy] benzoate (abbreviated ClPbis10BB, chemical structure shown in Fig. 1) [16]. We utilized the complementary techniques of dynamic light scattering and magnetic and electric field-induced orientational deformations (Freedericksz transitions), and focused on a single temperature within the (uniaxial) nematic range of a compound that has been extensively studied and is known to exhibit a number of the interesting properties listed above. Our principal results are the following: For the ratio of elastic constants, we find $K_{11}/K_{33} = 3.5$ (confirming the reversal in anisotropy recorded on a different bent-core compound in Ref. [12]) and $K_{11}/K_{22} = 10$ (∼6 times the ratio in typical calamitics), with $K_{11} = 3.1 \times 10^{-12}$ N. For the associated viscosities, we find $\eta_{\text{splay}}/\eta_{\text{twist}} = 3.0$ and $\eta_{\text{bend}}/\eta_{\text{twist}} = 3.2$ with $\eta_{\text{twist}} = 0.37$ Pa s. The viscosity ratios also contrast markedly with ordinary calamitics, where $\eta_{\text{twist}} > \eta_{\text{splay}}, \eta_{\text{bend}}$ due to the well-known backflow effect [17], and where all three viscosities are substantially smaller compared to the BCN. Motivated in part by recent small angle x-ray scattering measurements [18–20], we argue that the unusual results for the elastic or viscous parameters in the BCN stem from short-range smectic order similar to the polar layer structure that is characteristic of the smectic-*CP* phases of bent-core mesogens.

II. EXPERIMENTAL APPROACH

Standard sandwich cells with rubbed polyimide alignment layers on top of ITO electrodes were filled in the isotropic phase with the bent-core LC ClPbis10BB or the standard calamitic 4-pentyl-4′-cyanobiphenyl (5CB), which was used as a control in order to establish the accuracy of our measurements of elastic constants and orientational viscosites relative to literature values [21]. The sample thicknesses were 10 μm and 27 μm for the light scattering and Freedericksz transition measurements, respectively. After the cells were loaded, they were slowly cooled below the isotropic-nematic transition ($T_{IN} = 76$ °C for ClPbis10BB and 35 °C for 5CB), and polarizing microscopy was used to confirm high-quality homogeneous alignment of the nematic director. All subsequent measurements were performed at $T_{IN} - T = 2$ °C for ClPbis10BB or 12 °C for 5CB.

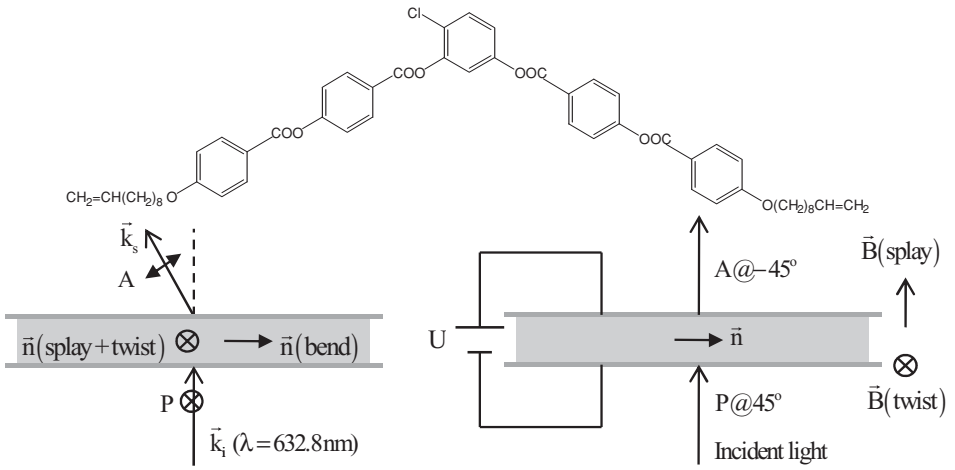

FIG. 1. Molecular structure of ClPbis10BB, and schematics of the sample geometries used in the light scattering (left) and Freedericksz transition (right) measurements.

A. Light scattering

In the light scattering experiments, samples were illuminated with a helium-neon laser (Spectra-Physics, model 127) with typical incident power of 1 mW, wavelength $\lambda_0 = 633$ nm, and polarization perpendicular to the scattering plane. The samples were held in a cylindrical aluminum oven with optical access covering a $0^\circ - 160^\circ$ angular range. Time correlation functions of the depolarized scattered intensity were recorded using a commercial electronic correlator (Flexible Instruments, model Flex2K-12Dx2).

We utilized two standard nematic scattering geometries, shown schematically in Fig. 1: the "splay + twist" geometry, where pure splay and pure twist fluctuation modes contribute simultaneously, and the "twist-bend" geometry in which a single mode (combining twist and bend elastic distortions) contributes. In the case of splay + twist, the scattering vector $\vec{q}$ is in the plane perpendicular to the average director $\vec{n}$ ($\vec{q} = \vec{q}_\perp$). Taking $\vec{n} = \hat{z}$ and $\hat{x}$ as the direction of normally incident light, we have $\vec{q}_\perp = (2\pi/\lambda_0)[(\sqrt{n_\perp^2 - \sin^2\theta_l} - n_\parallel)\,\hat{x} - \sin\theta_l\,\hat{y}]$, where $n_\perp$, $n_\parallel$ are the refractive indices for light polarized perpendicular or parallel to $\vec{n}$, and θ_l is the laboratory scattering angle. The scattering amplitudes for the two modes are given by

$$A_1 = I_0 \frac{\epsilon_a^2}{\epsilon_0^2} \frac{V k_B T G_1}{K_{11} q_\perp^2}, \quad A_2 = I_0 \frac{\epsilon_a^2}{\epsilon_0^2} \frac{V k_B T G_2}{K_{22} q_\perp^2}, \tag{1}$$

where I_0 is the incident laser intensity, V is the illuminated sample volume, and ϵ_a is the dielectric anisotropy at the laser line frequency. The geometrical factors G_1, G_2 may be calculated from standard expressions for nematic director mode scattering [22],

$$G_1 = \frac{n_\parallel^2}{n_\perp^2} \left(\frac{\sin^2\theta_l}{n_\perp^2 + n_\parallel^2 - 2n_\parallel\sqrt{n_\perp^2 - \sin^2\theta_l}} \right),$$

$$G_2 = \frac{\left(n_\perp - \frac{n_\parallel}{n_\perp}\sqrt{n_\perp^2 - \sin^2\theta_l}\right)^2}{n_\perp^2 + n_\parallel^2 - 2n_\parallel\sqrt{n_\perp^2 - \sin^2\theta_l}}. \tag{2}$$

The corresponding relaxation rates are

$$\Gamma_1 = \frac{K_{11} q_\perp^2}{\eta_{\text{splay}}}, \quad \Gamma_2 = \frac{K_{22} q_\perp^2}{\eta_{\text{twist}}}. \tag{3}$$

In the twist-bend geometry, $\vec{n}$ lies in the scattering plane, and we have $\vec{q} = (2\pi/\lambda)[(n_\parallel\sqrt{n_\perp^2 - \sin^2\theta_l}/n_\perp - n_\perp)\,\hat{x} - \sin\theta_l\,\hat{z}]$ and

$$A_3 = I_0 \frac{\epsilon_a^2}{\epsilon_0^2} \frac{V k_B T G_3}{K_{33} q_z^2}, \quad \Gamma_3 = \frac{K_{33} q_z^2}{\eta_{\text{bend}}}, \tag{4}$$

where

$$G_3 = \frac{n_\perp^2 - \sin^2\theta_l}{n_\perp^2 + (n_\perp^2/n_\parallel^2 - 1)\sin^2\theta_l}. \tag{5}$$

In Eq. (4), we neglected the contribution of twist; its ratio to the bend component is $K_{22} q_x^2 / K_{33} q_z^2$. For the range of θ_l probed, and characteristic values of $n_\perp$, $n_\parallel$ in the nematic phase of ClPbis10BB, we calculate the maximum $q_x^2/q_z^2 \simeq 0.10$. Since our results for the elastic constants [which are presented below and which do not rely on the approximation in Eq. (4)] indicate that $K_{22}/K_{33} \simeq 0.35$, we estimate that the maximum $K_{22} q_x^2 / K_{33} q_z^2 \lesssim 0.03$, i.e., the twist contribution to A_3 and Γ_3 is negligible.

The director fluctuation modes in nematics are overdamped. Thus time correlation data from splay + twist scattering should be analyzed by two decaying exponentials, or one in the case of twist-bend. This analysis yields the relative mode amplitudes and the mode relaxation rates. From the slope of the relaxation rates in Eqs. (3) and (4), we may obtain the parameters $K_{11}/\eta_{\text{splay}}$, $K_{22}/\eta_{\text{twist}}$, and $K_{33}/\eta_{\text{bend}}$, while the ratio of twist and splay amplitudes in Eqs. (1) gives

$$\frac{A_2}{A_1} = \frac{K_{11}}{K_{22}} \frac{G_2}{G_1}. \tag{6}$$

B. Freedericksz transitions

In our Freedericksz transition (FT) studies, 27-μm-thick homogeneously aligned samples of ClPbis10BB (or 5CB) were placed in a temperature-regulated oven that could be mounted between the pole faces of a large electromagnet in two alternative orientations, where the applied field $\vec{B}$ is perpendicular to $\vec{n}$ in both cases, and $\vec{B}$ is either in the plane of the substrates or across the cell gap and normal to the substrates (Fig. 1). The former geometry corresponds to a field-induced splay-bend deformation, and the latter to a pure twist distortion of the director. A 4-mW HeNe laser, normally incident on the sample (with $\vec{k} \perp \vec{n}$), together with a polarizer-analyzer combination and amplified photodetector (Thorlabs, model PDA55), were used to detect optically the threshold field B_t for the onset of these deformations. The magnetic field, recorded with a small Hall probe mounted near the sample, could be adjusted continuously from 0 to 1.3 T, and was highly uniform over the sample cell volume. Since the permeability μ of the liquid crystal is essentially identical to μ_0, the measured B is basically equal to B in the sample. During all experiments, the temperature was stable within 0.05 °C of the set value.

For the splay-bend FT experiment, the polarizer and analyzer were oriented at $\pm 45^\circ$ with respect to $\vec{n}$, producing the maximum in transmitted light intensity at zero field. The splay threshold was then detected by a drop in intensity with increasing field. The field was typically stepped in 1 mT increments, with a pause after each step to allow the measured intensity to stabilize fully. In addition to the optical transmission data, the cell capacitance was also recorded as a function of applied B using a precision capacitance bridge (Andeen-Hagerling, model 2500A) with a probe voltage of 0.1 V at 1 kHz frequency. Finally, using the optical transmission method, we also determined the change in B_t as a function of an ac voltage (1 kHz frequency, rms amplitude U ranging from 0 to 3 V), which was applied across the sample (i.e., electric field normal to the undistorted $\vec{n}$).

The measurements made in the splay-bend FT geometry were analyzed using well-known theoretical predictions for an aligned uniaxial nematic. Here we will simply quote the relevant results, which are comprehensively reviewed in the literature [23]. The forward transmitted light intensity I (assuming negligible absorption and scattering loss) between the crossed polarizer and analyzer may be expressed as

$$I = I_0 \sin^2\left(\frac{\Delta\phi}{2}\right) \sin^2 2\alpha, \tag{7}$$

where I_0 is the incident light intensity, $\alpha = 45^\circ$ is the angle between the polarizer and the undistorted $\vec{n}$, and $\Delta\phi$, the phase shift between ordinary and extraordinary waves, is given by

$$\Delta\phi = \frac{4Ln_e}{\lambda}\frac{B_t}{B}\int_{\xi_0}^{\pi/2} \sqrt{\frac{1+\kappa \sin^2\vartheta_m \sin^2\xi}{1-\sin^2\vartheta_m \sin^2\xi}} \times \left(\frac{1}{\sqrt{1+\nu \sin^2\vartheta_m \sin^2\xi}} - \frac{1}{\sqrt{1+\nu}}\right) d\xi. \tag{8}$$

Here $L = 27\mu$m is the sample thickness, $\lambda = 633$ nm is the optical wavelength, $\kappa = K_{33}/K_{11} - 1$, and $\nu = (n_e^2 - n_o^2)/n_o^2$, with $n_o = n_\perp$ and $n_e = n_\parallel$ being the ordinary and extraordinary refractive indices, respectively, for normally incident light. The parameter ξ_0 is given by $\xi_0 = \sin^{-1}(\sin\vartheta_0/\sin\vartheta_m)$, where ϑ_0 is the surface pretilt angle and ϑ_m is the (maximum) tilt angle in the middle of the cell. This angle may be calculated from the equation,

$$\frac{\pi}{2}\frac{B}{B_t} = \int_{\xi_0}^{\pi/2} \sqrt{\frac{1+\kappa \sin^2\vartheta_m \sin^2\xi}{1-\sin^2\vartheta_m \sin^2\xi}}\, d\xi. \tag{9}$$

The expression for the effective dielectric constant extracted from our capacitance measurements in the presence of applied B is

$$\frac{\epsilon_{\rm eff}}{\epsilon_0} = \frac{\pi}{2}\frac{B}{B_t}\left[\int_{\xi_0}^{\pi/2} \sqrt{\frac{1+\kappa \sin^2\vartheta_m \sin^2\xi}{(\epsilon_\perp + \epsilon_a \sin^2\vartheta_m \sin^2\xi)^2(1-\sin^2\vartheta_m \sin^2\xi)}}\, d\xi\right]^{-1}, \tag{10}$$

where $\epsilon_a = \epsilon_\parallel - \epsilon_\perp$ is the dielectric anisotropy at the 1 kHz frequency used in our experiment. Finally, the threshold magnetic field in the presence of an applied voltage (amplitude U) is determined by

$$\frac{B_t}{B_0} = \sqrt{1 \mp \left(\frac{U}{U_0}\right)^2}, \tag{11}$$

where the $-$ and $+$ signs apply to the cases $\epsilon_a > 0$ and $\epsilon_a < 0$, respectively, and

$$B_0 = \frac{\pi}{L}\sqrt{\frac{\mu_0 K_{11}}{|\chi_a|}}, \quad U_0 = \pi\sqrt{\frac{K_{11}}{|\epsilon_a|}}. \tag{12}$$

It is clear that by measuring $\Delta\phi$ [from the transmitted intensity I via Eq. (7)] and $\epsilon_{\rm eff}/\epsilon_0$ as functions of B, then determining B_t as a function of U, and finally analyzing the data using Eqs. (8)–(12), one can obtain values for the ratio K_{33}/K_{11}, the dielectric constant $\epsilon_\perp/\epsilon_0$, the dielectric anisotropy $|\epsilon_a/\epsilon_0|$, the elastic constant K_{11}, and the diamagnetic susceptibility anisotropy χ_a. Details will be given in the following section.

In the twist FT geometry ($\vec{B} \perp$ undistorted $\vec{n}$ and $\chi_a > 0$), the polarizer and analyzer axes were set at 0° and 90° with respect to the initially uniform $\vec{n}$, corresponding to zero transmitted optical intensity in the undistorted state. Since the sample thickness L greatly exceeds the optical wavelength λ, the optical transmission measurement is carried out in the Mauguin limit, so that in the case of twist and

at normal incidence, the light polarization simply follows the director orientation, and both the net phase shift across the sample between ordinary and extraordinary waves and the depolarized transmitted intensity remain at the minimum values through the onset of the field-induced deformation. Here, to detect the transition, we monitored the intensity of the depolarized light *scattered* in a narrow cone about the forward direction. Our measurements were done without any applied electric field, so that the threshold magnetic field is given by

$$B_t = \frac{\pi}{L}\sqrt{\frac{\mu_0 K_{22}}{|\chi_a|}}. \tag{13}$$

Combining this measurement with the results from the splay geometry (specifically, the value obtained for $|\chi_a|$), we can deduce the value of K_{22}. Note that the results from the FT experiments can then be checked for consistency with the light scattering results by comparing the ratio K_{22}/K_{11} obtained from the two techniques. Once the elastic constants are determined, the orientational viscosities may be calculated, via Eqs. (3) and (4), from the light scattering data for the relaxation rates of the director fluctuation modes.

III. RESULTS

We first consider our light scattering results. Figure 2 displays typical intensity correlation data obtained on ClPbis10BB at $T_{IN} - T = 2\,^{\circ}$C in the splay + twist and twist-bend geometries. In the former case, where two modes (pure splay and pure twist) are anticipated, the figure insets show

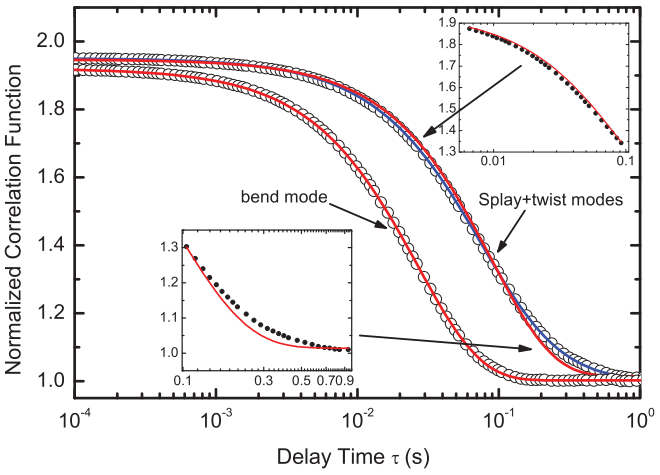

FIG. 2. (Color online) Typical light scattering correlation functions taken on a homogeneously aligned, 10-μm-thick sample of ClPbis10BB at $T_{NI} - T = 2\,^{\circ}$C. Main figure, right: Result for pure splay + pure twist geometry, with $q_\perp = 18\,700$ cm^{-1}, $q_z = 0$. The solid line passing directly through all the data points (open circles) is a fit to a double exponential decay, representing the two expected overdamped director modes. An additional line represents the best fit to a single exponential decay, which, as highlighted in the insets, does not accurately describe the data (solid dots). Main figure, left: Result for nearly pure bend geometry, with $q_z = 49\,600$ cm^{-1}, $q_\perp = 2300$ cm^{-1}. The solid line is an accurate fit to a single exponential decay.

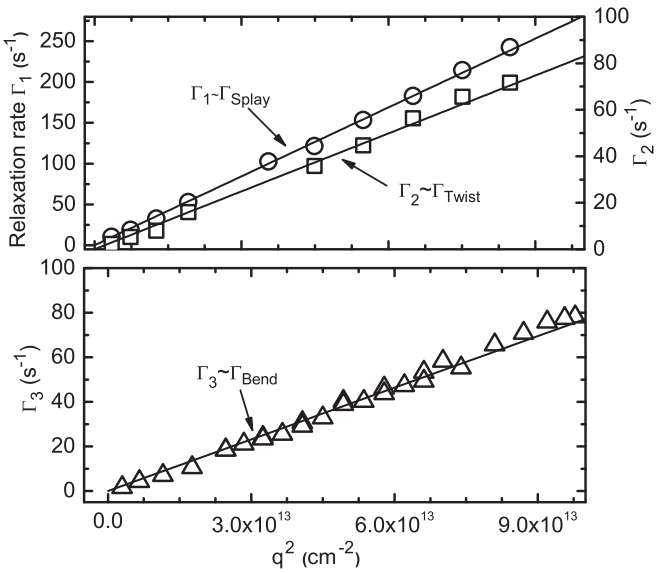

FIG. 3. Dispersion of the relaxation rates associated with splay, twist, and bend fluctuations of the director in ClPbis10BB at $T_{IN} - T = 2\,^{\circ}$C. The slopes of the lines give the corresponding elastic constant to viscosity ratios.

that a single exponential fit is clearly unsatisfactory. On the other hand, a fit to two decays describes the data well. For the twist-bend geometry, fitting to a single mode suffices, as expected. Our results for the dispersion of the relaxation rates Γ_{splay}, Γ_{twist}, and Γ_{bend} are presented in Fig. 3. These have the expected linear-in-q^2 dependence, and the fits to Eqs. (3) and (4) give the values of $K_{11}/\eta_{\text{splay}}$, $K_{22}/\eta_{\text{twist}}$, and $K_{33}/\eta_{\text{bend}}$ listed in Table I, together with our results and literature values [21] for the control compound 5CB. Evidently, the elasticity to viscosity ratios are significantly lower in the BCN compared to a standard calamitic, even when the nematic range of the latter exists at lower temperature.

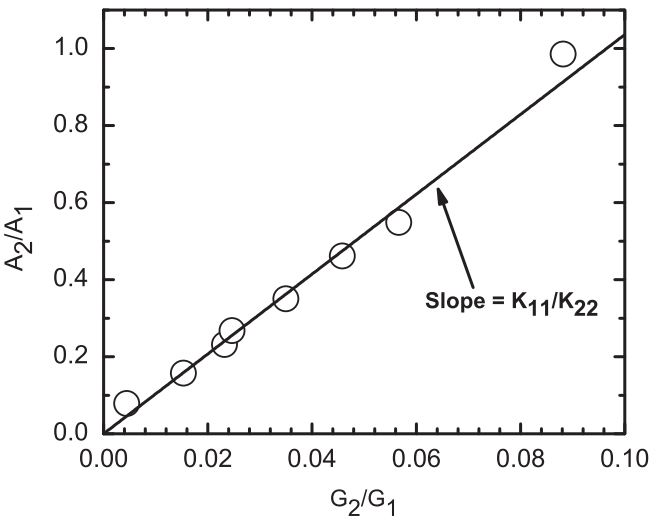

FIG. 4. Ratio of mode amplitudes, obtained from fitting of the correlation data in the splay + twist light scattering geometry for ClPbis10BB, plotted against the ratio of geometric factors calculated from Eq. (2) ($T_{IN} - T = 2\,^{\circ}$C). Slope gives the ratio of splay to twist elastic constants [see Eq. (6)].

TABLE I. Summary of measurements of elasticities and viscosities in our BCN compound at $T_{IN} - T = 2\,^{\circ}$C and the calamitic control compound 5CB at $T_{IN} - T = 12\,^{\circ}$C. LS, FT, and C label quantities obtained in this work from dynamic light scattering, Freedericksz transition techniques, or by combining results of the two.

Parameter	ClPbis10BB (this work)	5CB (this work)	5CB (Ref. [21])
$K_{11}/\eta_{\text{splay}}$ (m^2 s^{-1}) (LS)	2.8×10^{-12}	6.1×10^{-11}	7.2×10^{-11}
$K_{22}/\eta_{\text{twist}}$ (m^2 s^{-1}) (LS)	0.83×10^{-12}	3.2×10^{-11}	4.0×10^{-11}
$K_{33}/\eta_{\text{bend}}$ (m^2 s^{-1}) (LS)	0.77×10^{-12}	42×10^{-11}	45×10^{-11}
K_{11}/K_{33} (FT)	3.5	0.68	0.69
K_{11}/K_{22} (LS,FT)	10	1.6	1.7
K_{11} (N) (FT)	3.1×10^{-12}	5.9×10^{-12}	6.7×10^{-12}
K_{22} (N) (FT,C)	0.31×10^{-12}	3.7×10^{-12}	3.8×10^{-12}
K_{33} (N) (FT)	0.88×10^{-12}	8.7×10^{-12}	9.4×10^{-12}
η_{splay} (Pa s) (C)	1.1	0.097	0.093
η_{twist} (Pa s) (C)	0.37	0.12	0.095
η_{bend} (Pa s) (C)	1.2	0.021	0.021

In Fig. 4, we plot the amplitude ratio A_2/A_1 versus G_2/G_1 for ClPbis10BB; the fit to Eq. (6) yields $K_{11}/K_{22} = 10$, which is significantly larger than the value of 1.6 that we obtained for 5CB (which is also quite typical of other calamitic nematics).

Our major results from the FT measurements are illustrated in Figs. 5–7 and summarized in Table I. Figure 5 (top panel) displays data for the effective dielectric constant of the ClPbis10BB sample as a function of magnetic field B at $T_{IN} - T = 2\,^{\circ}$C. The threshold field for the onset of a splay distortion corresponds to the dropoff in $\epsilon_{\text{eff}}/\epsilon_0$ from its initial plateau; the noticeable rounding of the plateau reflects a finite pretilt (angle ϑ_0) of the director at the cell surfaces. As the solid line indicates, the data (including that for values of B beyond the threshold, where the distortion involves a mixture of splay and bend) are fitted quite well by the theoretical expression in Eq. (10). In the fit, the parameter $\epsilon_\perp$ was fixed to the value read off from the low-field plateau, $\epsilon_\perp = 6.4\epsilon_0$, while B_t, ϑ_0, $\epsilon_\parallel$, and κ were varied, starting with order-of-magnitude initial estimates of their values. The bottom panel in Fig. 5 shows typical data for the optical phase shift as a function of applied field, deduced from our transmitted light intensity measurements using Eq. (7). The solid curve is a fit to Eq. (8), with variable parameters B_t, $n_\parallel$, $n_\perp$, and κ. The fit for $\epsilon_{\text{eff}}/\epsilon_0$ yields $\vartheta = 0.06$ rad, $\epsilon_\parallel = 5.2\epsilon_0$ (which, combined with $\epsilon_\perp = 6.4\epsilon_0$, gives $\epsilon_a = -1.2\epsilon_0$ at low frequency), while

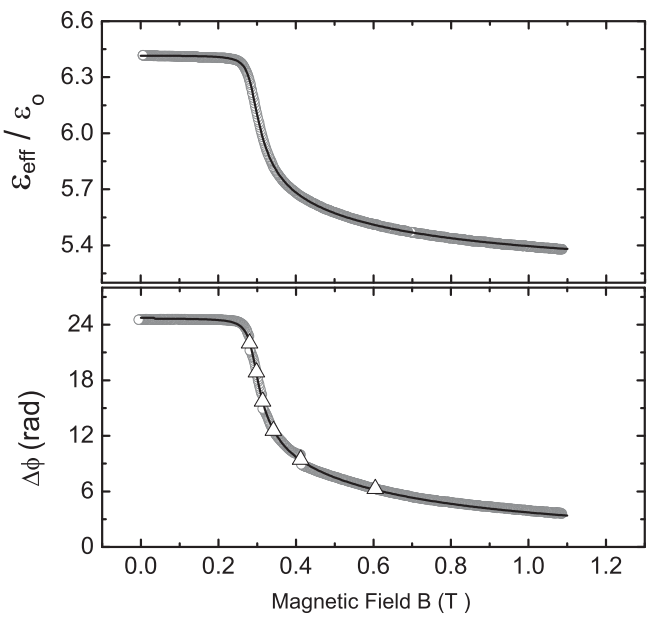

FIG. 5. Top panel: Effective dielectric constant of ClPbis10BB measured as a function of applied magnetic field B in the "splay" Freedericksz geometry and for $T_{IN} - T = 2\,^{\circ}$C. The vertical axis intercept corresponds to the value of $\epsilon_\perp/\epsilon_0$. The solid line is a fit to Eq. (10) of the text. Bottom: Data for the phase shift $\Delta\phi$ between ordinary and extraordinary components of polarized light transmitted through the sample as a function of applied B. The solid line is a fit to Eq. (8). The triangular symbols correspond to values of $\Delta\phi$ where the intensity in Eq. (7) is a maximum.

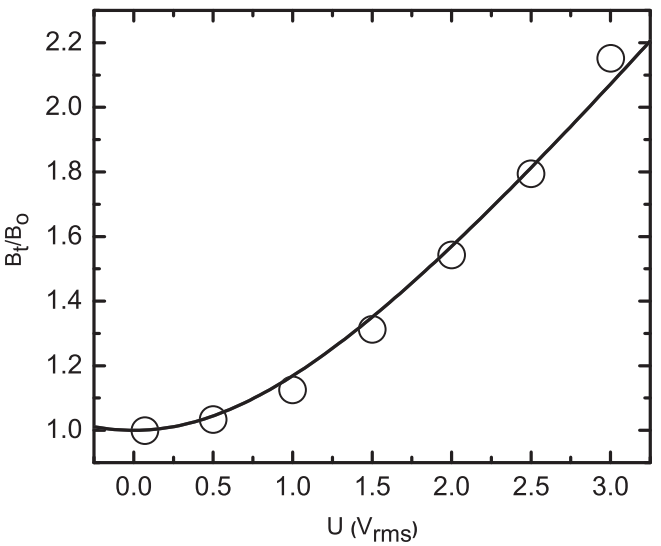

FIG. 6. Threshold magnetic field for splay-bend Freedericksz transition in ClPbis10BB determined as a function of voltage applied across the sample cell ($T_{IN} - T = 2\,^{\circ}$C). The E and B fields are parallel to each other and normal to the undistorted director. The solid line is a fit to Eq. (11) in the text.

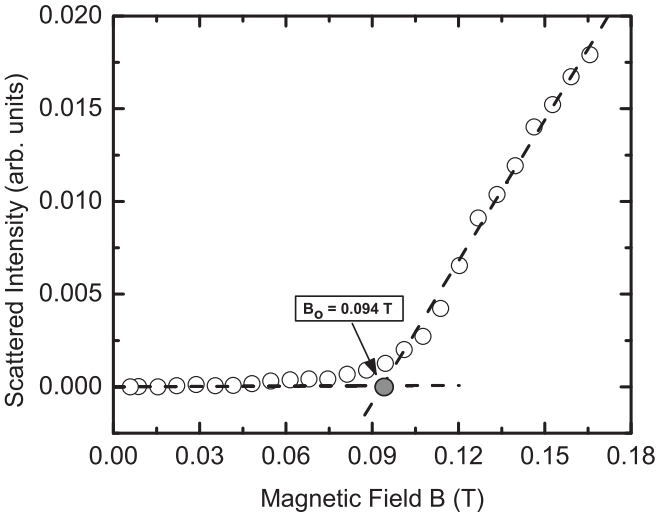

FIG. 7. Intensity of depolarized scattered light collected from the ClPbis10BB sample for small angles off the incident direction and plotted against applied magnetic field in the twist Freedericksz geometry. The dashed lines are used to estimate the threshold field for a twist distortion of the director. (Temperature $T_{IN} - T = 2\,^{\circ}$C.)

the fit for $\Delta\phi$ gives $n_{\parallel} = 1.64$ and $n_{\perp} = 1.55$ at optical frequency [24]. The two fits produce identical values (to two significant figures) of $B_t = 0.30$ T and $\kappa = -0.72$.

Figure 6 displays results for the threshold field B_t for ClPbis10BB measured for various voltages (amplitude U, frequency 1 kHz) applied across the sample cell. The solid curve is a fit to Eq. (11) with $B_0 = 0.30$ T and the single variable parameter U_0, for which we obtain $U_0 = 1.7$ V. We can now check for the possible effect on the value of B_0 (fixed in the fit) due to the 0.1 V, 1 kHz probe voltage used to measure the sample capacitance. Setting $U = 0.1$V and $U_0 = 1.7$ V in Eq. (11), we get $B_t = 1.002B_0$, a difference which is negligible. Now using $U_0 = 1.7$ V, $L = 27$ μm, and the value of $\epsilon_a = -1.2\epsilon_0$ (see above), we calculate $K_{11} = 3.1 \times 10^{-12}$ N from Eq. (12), and then from the parameter $\kappa = K_{33}/K_{11} - 1 = -0.72$, we get $K_{33} = 0.88 \times 10^{-12}$ N. Further, with $B_0 = 0.30$ T and using the appropriate expression in Eq. (12), we calculate $\chi_a = 5.8 \times 10^{-7}$.

Next we turn to our results for the twist Freedericksz transition; a typical measurement for ClPbis10BB (again at $T_{IN} - T = 2\,^{\circ}$C) is shown in Fig. 7, where the small-angle scattered intensity is plotted against field B (applied perpendicular to the initial director orientation). By extrapolating the initial linear increase of the signal to zero (see the dashed line in the figure), we identify the threshold field as $B_t = 0.094$ T, and then from Eq. (13) and the value of χ_a obtained above, we find $K_{22} = 0.31 \times 10^{-12}$ N.

Table I collects our main experimental results for both the bent-core nematic (ClPbis10BB) and the calamitic control (5CB) samples, with literature values included for the latter. The entries for the viscosities were obtained by combining the light scattering data for the elasticity-viscosity ratios with the elastic constants determined from the FT measurements. Our estimated error on the individual values of K and η is $\pm 10\%$. Within this error bar, we find good agreement between our measurement of these parameters and the literature values for 5CB, validating our implementation of the combined LS and FT techniques.

IV. DISCUSSION

The results in Table I clearly demonstrate that while the nematic phase of our bent-core compound has uniaxial symmetry similar to ordinary uniaxial calamitics, its viscoelastic parameters are profoundly different. Specifically, the elastic constant K_{33} is about three times smaller than K_{11}—nearly the reverse of calamitics, where K_{33} is typically almost twice as large as K_{11}—and K_{22} is one order of magnitude smaller than the typical value in ordinary calamitics. We also observe a dramatic enhancement of the viscosities for director fluctuations compared to rodlike thermotropic liquid crystals. The twist viscosity is $\sim$4 times higher, and the splay and bend viscosities are 10 to 100 times greater than the usual values for calamitics. Quite striking is the finding that η_{twist} is smaller than both η_{splay} and η_{bend}, which is the opposite of what is ordinarily observed in calamitics, where backflow effects tend to reduce the latter relative to the former.

Let us first discuss the reduction of K_{33} relative to K_{11}. Based on a molecular statistical theory, Helfrich predicted a decrease in K_{33} for bent-shaped mesogens given by [25]

$$K_{33} = \frac{\bar{K}_{33}}{1 + \beta^2 N^{-1/3} \bar{K}_{33}/2k_B T}, \tag{14}$$

where β is the molecular bend angle, $\bar{K}_{33}$ is the bend elastic constant when $\beta = 0$ (as for a rodlike molecule), and N is the molecular number density. In the theory, the splay constant K_{11} is not supposed to be affected by the molecular bend, so $K_{11} \approx \bar{K}_{11}$. Taking typical values $\beta \sim 1$ rad, $N \sim 10^{27}$ m^{-3}, $T = 350$ K, and $\bar{K}_{33} = 10 \times 10^{-12}$ N, we get $K_{33} \approx \bar{K}_{33}/2$. This explains part but not all of the observed reduction in K_{33}/K_{11}. In addition, Helfrich's model does not predict any decrease in K_{22}, whereas we found approximately one order of magnitude decrease there, too.

A satisfactory explanation of the significantly lower twist and bend constants relative to calamitics requires a model that not only takes into account the molecular shape, but also the potential effects of local correlations among molecules of reduced symmetry that may exist in the nematic state. Recent small angle x-ray scattering studies on ClPbis10BB and similar BCNs [18–20], together with earlier light scattering experiments [6], indicate the presence of short-range, smectic-C correlated molecular "clusters" throughout the nematic range, which exist even in the absence of a lower temperature smectic phase and are characterized by nearly temperature-independent correlation lengths comparable to a few molecular lengths. The presence of these clusters has also been invoked to explain other observations, such as non-Newtonian flow characteristics [26] and certain remarkable aspects of shear-induced birefringence [27]. For our discussion here, the most interesting possibility is that the clusters might be chiral. It is well known that the smectic-C phases of bent-core LCs are typically composed of polar layers (hence designated smectic-CP), with the bow directions arranged either ferro- or antiferroelectrically between layers, and the tilt directions

(in the plane normal to the bow) either the the same (synclinic) or alternating (anticlinic). In two particular combinations, ferrolectric-synclinic and antiferroelectric-anticlinic, the layer structure is chiral (even if the constituent molecules are not) and the system forms a racemic mix of right- and left-handed chiral domains (both signs of the layer chirality being equally likely). These chiral domains can be either a minority [28] or majority [29] component in bent-core smectics. If, analogously, a distribution of short-range correlated, chiral smecticlike clusters is present in a bent-core nematic, the system could be softened with respect to *both* twist and bend distortions, since chiral stacking of tilted smectic clusters naturally involves a combination of molecular twist and bend [30]. The overall result could then be a significant reduction in the bulk K_{22} and K_{33} relative to K_{11}. Moreover, if the opposite chiral "enantiomers" occur with equal probability, the BCN exhibits no macroscopic chirality, as we have indeed concluded from polarizing microscopy on ClPbis10BB. Interestingly, dielectric spectroscopy [31] reveals a slow relaxation process in ClPbis10BB, which was not observed in a related calamitic compound and might result from rotation of polar (ferroelectric) molecular aggregates.

The anisotropy of the orientational viscosities in our BCN is even more unusual than that of the elastic constants. The main result $\eta_{\text{splay}} \simeq \eta_{\text{bend}} > \eta_{\text{twist}}$ depends critically on our measurement of K_{22} (which is then combined with the elasticity to viscosity ratio from light scattering to obtain η_{twist}). As we pointed out earlier, the twist constant is the most challenging to measure by the Freedericksz transition method; however, we have at least two independent indications that our result is accurate. First, the ratio K_{11}/K_{22}, as determined from light scattering, agrees completely with the value calculated from the twist and splay FT data. Second, as referred to in the Introduction, other experimental methods, namely optical observations of electric field-induced splay domains separated by Brochard-Leger walls in a BCN [14], also indicate that the twist constant is as much as ten times smaller than the other elastic constants.

In conventional nematohydrodynamics, the coupling of flow to rotation of the director ("backflow") reduces the effective viscosities for bend and for splay relative to twist distotions [17]; apparently, the opposite occurs in the BCN. It is also known that the flow behavior of bent-core LCs differs qualitatively from rodlike nematics. The former exhibit a finite yield stress similar to Bingham fluids [26], i.e., no flow below a threshold applied shear stress. If one sets the velocity gradients to zero—or takes the limit of no flow—in the standard Erickson-Leslie-Parodi (ELP) model of the dissipation, all of the orientational viscosities simply collapse onto a pure rotational coefficient $\gamma_1 = \alpha_3 - \alpha_2$ (following the ELP notation). While this eliminates the reduction in η_{splay} and η_{bend} due to backflow, it also indicates that the ELP model cannot give values above η_{twist}. One can also consider the impact of the short-range smectic order on the dissipative behavior. Smectic order parameter fluctuations and defect motion are known to produce interesting dynamical effects such as sign reversal of the Leslie coefficient α_3 [32], finite yield threshold in the shear flow of smectic layers at low stresses [33], and shear thinning [34]. Yet none of these has been associated with a *nematic* far from any transition to a smectic phase. An alternative possibility, based on the model of a BCN suggested above, is an additional dissipation mechanism arising from the presence of metastable, smecticlike molecular clusters, which are separated on average by fluidlike (or "melted") regions. Specifically, we suggest that splay or bend distortions of the average director of the clusters are coupled to local deviation in their equilibrium distribution or perhaps even their size or internal configuration. If such a coupling actually reduces the entropy of the system, then one may expect that the splay and bend viscosities will be shifted upward from their "bare" value, in order to guarantee net entropy production by the associated fluctuations. This shift is opposite to the usual nematic backflow effect, where induced flow provides additional dissipation. We further conjecture that, the distribution of the clusters would not change under a pure rotation, so the twist viscosity is not selectively enhanced. Of course, a substantial concentration of smectic-like clusters should significantly elevate all of the viscosities relative to the values in standard calamitic nematics, as we have observed.

V. CONCLUSION

We measured the orientational elastic constants and associated viscosity coefficients of a bent-core nematic liquid crystal. In addition to quantitative disparities (most dramatic in the magnitude of the viscosities), we found qualitative differences in the anisotropy of these parameters between the BCN and conventional calamitic nematics. Our proposed explanation of the differences is based on structural evidence [18–20] that, while the macroscopic symmetry of the nematics is similar, the BCN is characterized by a random distribution of nanoscale molecular clusters with tilted smectic correlations. The potential chirality of such clusters, or of a minority of them acting effectively as chiral dopants, may selectively soften K_{22} and K_{33} relative to K_{11}. In addition, we suggested that the effect of the clustering on the dynamical dissipation may enhance the splay and bend viscosities relative to twist, as splay and bend distortions could require a reconfiguration of the local cluster distribution and thereby incur an extra entropy penalty. It will be useful to perform measurements similar to those we have reported here on a wider range of bent-core compounds, in order to determine what molecular features give rise to the behavior of the elasticity and viscosity ratios we observed.

ACKNOWLEDGMENTS

The authors thank the NSF for support under Grants No. DMR-0606160 and No. DMR-0964765. M.M. and S.S. gratefully acknowledge funding from Department of Energy Grant No. ER46572. P.S. was partially supported by the Hungarian Research Fund OTKA under Grant No. K81250.

[1] J. Harden, B. Mbanga, N. Eber, K. Fodor-Csorba, S. Sprunt, J. T. Gleeson, and A. Jakli, Phys. Rev. Lett. **97**, 157802 (2006).

[2] S. Dhara, F. Araoka, M. Lee, K. V. Le, L. Guo, B. K. Sadashiva, K. Song, K. Ishikawa, and H. Takezoe, Phys. Rev. E **78**, 050701(R) (2008).

[3] J. A. Olivares, S. Stojadinovic, T. Dingemans, S. Sprunt, and A. Jakli, Phys. Rev. E **68**, 041704 (2003).

[4] B. R. Acharya, A. Primak, and S. Kumar, Phys. Rev. Lett. **92**, 145506 (2004).

[5] L. A. Madsen, T. J. Dingemans, M. Nakata, and E. T. Samulski, Phys. Rev. Lett. **92**, 145505 (2004).

[6] S. Stojadinovic, A. Adorjan, S. Sprunt, H. Sawade, and A. Jakli, Phys. Rev. E **66**, 060701(R) (2002).

[7] T. Niori, J. Yamamato, and H. Yokoyama, Mol. Cryst. Liq. Cryst. **409**, 475 (2004).

[8] E. Dorjgotov, K. Fodor-Csorba, J. T. Gleeson, S. Sprunt, and A. Jakli, Liq. Cryst. **35**, 149 (2008).

[9] D. Wiant, J. T. Gleeson, N. Eber, K. Fodor-Csorba, A. Jakli, and T. Toth-Katona, Phys. Rev. E **72**, 041712 (2005).

[10] D. Wiant, K. Neupane, S. Sharma, J. T. Gleeson, S. Sprunt, A. Jakli, N. Pradhan, and G. Iannacchione, Phys. Rev. E **77**, 061701 (2008).

[11] T. C. Lubensky and L. Radzihovsky, Phys. Rev. E **66**, 031704 (2002).

[12] P. Sathyanarayana, M. Mathew, Q. Li, V. S. S. Sastry, B. Kundu, K. V. Le, H. Takezoe, and S. Dhara, Phys. Rev. E **81**, 010702(R) (2010).

[13] B. Kundu, R. Pratibha, and N. V. Madhusudana, Phys. Rev. Lett. **99**, 247802 (2007).

[14] M.-G. Tamba, W. Weissflog, A. Eremin, J. Heuer, and R. Stannarius, Eur. Phys. J. E **22**, 85 (2007).

[15] M. R. Dodge, C. Rosenblatt, R. G. Petschek, M. E. Neubert, and M. E. Walsh, Phys. Rev. E **62**, 5056 (2000); M. R. Dodge, R. G. Petschek, C. Rosenblatt, M. E. Neubert, and M. E. Walsh, *ibid.* **68**, 031703 (2003).

[16] K. Fodor-Csorba, A. Vajda, G. Galli, A. Jakli, D. Demus, S. Holly, and E. Gacs-Baitz, Macromol. Chem. Phys. **203**, 1556 (2002).

[17] F. Brochard, Mol. Cryst. Liq. Cryst. **23**, 51 (1973).

[18] S. H. Hong, R. Verduzco, J. C. Williams, R. J. Twieg, E. DiMasi, R. Pindak, A. Jakli, J. T. Gleeson, and S. Sprunt, Soft Matter **6**, 4819 (2010).

[19] O. Francescangeli, V. Stanic, S. I. Torgova, A. Strigazzi, N. Scaramuzza, C. Ferrero, I. P. Dolbnya, T. M. Weiss, R. Berardi, I. Muccioli, S. Orlandi, and C. Zannoni, Adv. Funct. Mater. **19**, 2592 (2009).

[20] C. Keith, A. Lehmann, U. Baumeister, M. Prehm, and C. Tschierske, Soft Matter **6**, 1704 (2010).

[21] G. P. Chen, H. Takezoe, and A. Fukuda, Liq. Cryst. **5**, 341 (1989).

[22] P. G. deGennes and J. Prost, *The Physics of Liquid Crystals*, second edition (Clarendon Press, Oxford, 1993), Chap. 3.

[23] I. W. Stewart, *The Static and Dynamic Continuum Theory of Liquid Crystals: A Mathematical Introduction* (Taylor and Francis, London, 2004), Chap. 3.

[24] Note that the dielectric anisotropy (ϵ_a) is negative at low frequency (e.g., ~1 kHz), while the refractive index anisotropy and thus ϵ_a are positive at optical frequencies. Such a reversal in the sign of ϵ_a is characteristic of elongated liquid crystal molecules that have a negative static dielectric anisotropy. See D. Dunmur and K. Toriyama "Physical Properties : Optical Properties" in *Handbook of Liquid Crystals* Vol 1: Fundamentals, ed. by D. Demus, J. Goodby, G. W. Gray, H. W. Spiess, and V. Vill (Wiley-VCH, Weinheim, Germany, 2008), pp 231-252.

[25] W. Helfrich, Mol. Cryst. Liq. Cryst. **26**, 1 (1974).

[26] C. Bailey, K. Fodor-Csorba, J. T. Gleeson, S. N. Sprunt, and A. Jakli, Soft Matter **5**, 3618 (2009).

[27] C. Bailey, K. Fodor-Csorba, R. Verduzco, J. T. Gleeson, S. Sprunt, and A. Jakli, Phys. Rev. Lett. **103**, 237803 (2009).

[28] D. R. Link, G. Natale, R. Shao, J. E. Maclennan, N. A. Clark, E. Korblova, and D. M. Walba, Science **278**, 1924 (1997); D. M. Walba, "Ferroelectric Liquid Crystal Conglomerates" in *Materials-Chirality: Volume 24 of Topics in Stereochemistry*, edited by M. M. Green, R. J. M. Nolte, and E. W. Meijer (Wiley, New York, 2003), pp 457-518.

[29] G. Heppke, A. Jakli, S. Rauch, and H. Sawade, Phys. Rev. E **60**, 5575 (1999).

[30] S. T. Lagerwall, *Ferroelectric and Antiferroelectric Liquid Crystals* (Wiley-VCH, Weinheim, 1999).

[31] P. Salamon, N. Eber, A. Buka, J. T. Gleeson, S. Sprunt, and A. Jakli, Phys. Rev. E **81**, 031711 (2010).

[32] W. L. McMillan, Phys. Rev. A **9**, 1720 (1974).

[33] R. G. Horn and M. Kleman, Ann. Phys. (Paris) **3**, 229 (1978).

[34] C. Meyer, S. Asnacios, C. Bourgaux, and M. Kleman, Rheol. Acta **39**, 223 (2000).